Studying the road grip of firefighting and rescue motorcycles when moving straight

Vu Khac Bảy[a], Duong Van Tai[b], Hoang Son[b], Luong Anh Tuan[c*] and Hoang Nhan[a]

[a]*Faculty of Engineering and Technology (FET), Nguyen Tat Thanh University, Ho Chi Minh City 700000, Vietnam*
[b]*College of Electromechanical and Civil Engineering, Vietnam National University of Forestry, Hanoi, Vietnam*
[c]*Faculty of Fire Prevention, University of fire prevention and fighting, Hanoi, Vietnam*

A R T I C L E I N F O	A B S T R A C T
	A fire fighting and rescue motorcycle fitted with a fire fighting and rescue vehicle cluster on the vehicle's suspension will change the vehicle's center of gravity, affecting the vehicle's stability during travel. By modeling the kinematics in the planar motion of a two-wheeled motorcycle with 4 degrees of freedom, the paper has built a system of differential equations for the planar motion of the vehicle. Investigate the influence of the installation position of the vehicle cluster, the road surface collision, and the vehicle's speed on the loading and unloading of the vehicle in the process of moving in a straight line. The test results evaluate the reliability of the theoretical model.

1. Introduction

Vietnamese-made firefighting and rescue motorcycles are installed on the base Kawasaki W175 (Fig. 1), operating mainly in the old quarter due to the narrow and small streets.

Fig. 1. Fire fighting and rescue motorcycle

* Corresponding author.
E-mail addresses: luonganhtuan@daihocpccc.edu.vn   (L. A. Tuan)

On the vehicle, there are more firefighting and rescue equipment installed on the suspension of the vehicle, so the center of gravity of the vehicle changes, affecting the stability of the vehicle during movement to quickly approach the fire area. Due to the installation of firefighting and rescue equipment (later called the equipment cluster), the center of gravity is shifted to the rear of the vehicle. Along with the impact of obstacles on the road, when moving the vehicle, there is a phenomenon of shaking and loading the vehicle. For example, this may occur at high speed and when the front wheel does not contact the road surface.

The dynamics of single-road vehicles such as motorcycles is a broad topic. Authors such as (Cossalter, 2006; Sharp 1976,1985, 2001, 2004,2006, 2008, 2012) explain dynamic equilibrium equations and the importance of steering geometry. The evolution of motorcycle suspension over the years have been described and explained for the pros and cons of the fork as a front suspension (e.g. Hossack 1983, Cossalter et al. 2000 Benini C.et al. 2017). In addition there are some researches on shock absorbers (Mavroudakis, Eberhard 2007), influence of aerodynamic forces during vehicle movement (Marchesin et al. 2018, Sharma and 2012), frequency analysis of motorcycles in planar motion (Zanarini and Brugnoni 2012) and study of the movement of motorcycles taking into account the impact of the rider (Zhu et al. 2012, Chindamo et al. 2018).

In any of the aforementioned works a special dynamic model is used. For example, Cossalter (2006) gives a kinetic point of view by treating the suspension as a rigid block and the motorcycle can be defined as a spatial mechanism consisting of four pieces of hardware: (i) the rear assembly (frame) , (ii) saddle, tank and drivetrain group motor), (iii) front assembly (fork, handlebar and handlebar) and (iv) front wheel and rear wheel. These rigid blocks are connected by three rotating joints (steering shaft and two wheel axles) and contact the ground at two points at the wheels. With the above model, with the assumption that the tire rotates without slipping, the vehicle has 3 degrees of freedom corresponding to three main movements: (1) the reciprocating motion of the motorcycle (represented by the rotation of the rear wheel); (2) rolling motion around a straight line connecting the contact points of the tire on the road plane; and (3) steering motion.

Zanarini and Brugnoni (2012) presented a flat motion model of a motorcycle simulated by 5 pieces of hardware: Suspension block (including chassis, engine, driver, sliders) of the front fork), the lower fork of the front fork, the rear fork, the front wheel, the rear wheel. These parts are linked together through rotary joints and translational joints. Assuming the vehicle is moving at a constant speed and the tire does not slip, the vehicle has 4 degrees of freedom corresponding to four main movements: three vertical movements of the two-wheel centers of gravity and the center of mass of the suspension mass, one rotation about the horizontal axis (perpendicular to the vertical and forward direction of the vehicle) passing through the center of gravity of the suspension block.

In this paper, for the purpose of studying wheel traction while the vehicle is moving straight, a flat motion model with 4 degrees of freedom is used. However, unlike Zanarini and Brugnoni (2012), the four degrees of freedom here will be corresponded to four main movements: two vertical movements of the center of gravity of the suspension block and the center of gravity of the front wheels, two rotation movements about the horizontal axis passing through the center of gravity of the suspension block and the horizontal axis passing through the center of gravity of the rear fork. In addition, the vehicle moves with the rear wheel speed according to a known law. In this model, assuming that the motorcycle has a rigid frame, the suspension mechanism, the shock absorbing, and nonlinear elastic and absorbing properties for the tire and aerodynamic effects are taken into account. By design, the instrument cluster is installed with the motorcycle's suspension block. Due to the structure of the vehicle and the need to reserve a seat for the driver, the installation location of the instrument cluster can only be in a certain area. The establishment and investigation of the system of dynamic equations needs to find a reasonable location to install the instrument cluster. Furthermore, the range of weight values of the instrument cluster is determined such that the vehicle remains stable when move straight with the speed of less than 70km/h.

2. Kinetics in flat motion of motorcycle

2.1. Plane motion model

The flat motion model of the motorcycle is simulated by 5 pieces of hardware:

(1) suspension block (including chassis, engine, driver, fire and rescue vehicle assembly, and front fork slider), (2) lower fork of front fork, (3) rear fork, (4) front wheel and (5) rear wheel. These parts are linked together through rotary joints and translational joints. Elasticity and damping coefficient are defined as: C_{br}, k_{br} for the rear wheel and C_{bf}, k_{bf} for the front wheel. The rear and front shock absorbers have also elastic and damping coefficients of C_r, k_r and C_f, k_f as shown in Fig. 2.

Select the overall coordinate system with the origin located at the contact position between the rear tire and the road, the x-axis is in the forward direction of the vehicle, and the z-axis is up. With the coordinate system selected as above, the symbols of the centroids of the clusters and their coordinates at the initial time ($t=0$) and at the time of consideration t are illustrated in Table 1.
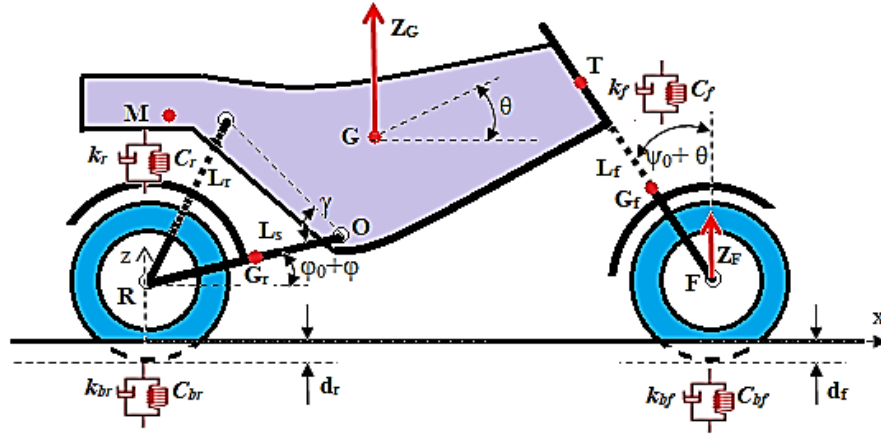
Fig. 2. Degrees of freedom and points of interest on the plane motion model of the vehicle

Table 1. Symbols of centroids, masses, initial coordinates and coordinates at time t of blocks

Content	Symbol	Mass	Initial coordinates	Coordinates at t
The center of mass includes: chassis, engine, driver, slider of the front fork.	G_n	m_{Gn}	$\left(x_{Gn}^0, z_{Gn}^0\right)$	$\left(x_{Gn}, z_{Gn}\right)$
The focus of the cluster of firefighting and rescue vehicles	M	m_M	$\left(x_M^0, z_M^0\right)$	$\left(x_M, z_M\right)$
Center of gravity suspension (including chassis, engine, driver, fire and rescue vehicle assembly, front fork slider)	G	m_G	$\left(x_G^0, z_G^0\right)$	$\left(x_G, z_G\right)$
Center of gravity of the cluster under the front fork	G_f	m_{Gf}	$\left(x_{Gf}^0, z_{Gf}^0\right)$	$\left(x_{Gf}, z_{Gf}\right)$
Center of gravity of the rear fork	G_r	m_{Gr}	$\left(x_{Gr}^0, z_{Gr}^0\right)$	$\left(x_{Gr}, z_{Gr}\right)$
Rear wheel center of gravity	R	m_R	$\left(x_R^0, z_R^0\right)$	$\left(x_R, z_R\right)$
Front wheel center of gravity	F	m_F	$\left(x_F^0, z_F^0\right)$	$\left(x_F, z_F\right)$

Moment of inertia about the axis parallel to O_y and passing through the center of gravity of the rotating blocks are: suspension block I_G, rear fork I_{Gr} and assembly under front fork I_{Gf}. The symbols d_r and d_f are the distance between the road surface and the rear and front tires. Thus, d_r and d_f are the settlement of the rear wheel and the front wheel (Fig. 2), so the front tire is in contact with the road surface when d_f is negative.

Considering the vehicle's motion in the plane of symmetry and assuming the vehicle is moving straight with the rear wheel velocity according to a known rule, the vehicle's kinematics can be analyzed by four degrees of freedom: displacement of G (weight) center of suspension) in the vertical direction Z, tilt angle θ of the suspension block in the longitudinal direction, displacement in the z direction of the front wheel and rotation angle φ of the rear fork. At the initial time: the rear fork OR is set up with the x-axis at an angle φ_0, the front fork is made with the z-axis with an initial angle of ψ_0 and the OS segment is made with an OR with an initial angle of γ_0. Thus, the system has four interpolated coordinates θ, φ, Z_G and Z_F to calculate. The pavement deformation function $z=f(x)$.

2.2. Displacement, kinetic energy, potential energy and dissipation function

Coordinates of points can be calculated through $\theta, \varphi, z_G, z_F, m_G = m_{Gn} + m_M$

at the beginning as:

$$x_G^0 = \frac{m_{Gn}x_{Gn}^0 + m_M x_M^0}{m_G}, \quad z_G^0 = \frac{m_{Gn}z_{Gn}^0 + m_M z_M^0}{m_G} \qquad (1)$$

Symbol:

$$\Delta_{OG} = \begin{pmatrix} x_O^0 - x_G^0 \\ z_O^0 - z_G^0 \end{pmatrix}, \quad \Delta_{GrO} = \begin{pmatrix} x_{Gr}^0 - x_O^0 \\ z_{Gr}^0 - z_O^0 \end{pmatrix}, \quad \Delta_{RO} = \begin{pmatrix} x_R^0 - x_O^0 \\ z_R^0 - z_O^0 \end{pmatrix}, \quad \Delta_{SG} = \begin{pmatrix} x_S^0 - x_G^0 \\ z_S^0 - z_G^0 \end{pmatrix},$$

$$\Delta_{GfF} = \begin{pmatrix} x_{Gf}^0 - x_F^0 \\ z_{Gf}^0 - z_F^0 \end{pmatrix}, \quad \Delta_{TG} = \begin{pmatrix} x_T^0 - x_G^0 \\ z_T^0 - z_G^0 \end{pmatrix}, \quad \Delta_{SR} = \begin{pmatrix} x_S^0 - x_R^0 \\ z_S^0 - z_R^0 \end{pmatrix}, \quad \Delta_{TF} = \begin{pmatrix} x_T^0 - x_F^0 \\ z_T^0 - z_F^0 \end{pmatrix} \tag{2}$$

$$A_1 = (\cos\theta \ -\sin\theta), \ A_2 = (\sin\theta \ \cos\theta), \ dA_1 = (-\sin\theta \ -\cos\theta), \ dA_2 = (\cos\theta \ -\sin\theta),$$
$$B_1 = (\cos\varphi \ -\sin\varphi), \ B_2 = (\sin\varphi \ \cos\varphi), \ dB_1 = (-\sin\varphi \ -\cos\varphi), \ dB_2 = (\cos\varphi \ -\sin\varphi)$$

Transpose matrices:

$$U_O = \begin{pmatrix} x_O \\ z_O \end{pmatrix}, U_G = \begin{pmatrix} x_G \\ z_G \end{pmatrix}, U_{Gr} = \begin{pmatrix} x_{Gr} \\ z_{Gr} \end{pmatrix}, \ U_R = \begin{pmatrix} x_R \\ z_R \end{pmatrix}, \ U_S = \begin{pmatrix} x_S \\ z_S \end{pmatrix}, U_{Gf} = \begin{pmatrix} x_{Gf} \\ z_{Gf} \end{pmatrix}, U_T = \begin{pmatrix} x_T \\ z_T \end{pmatrix} \tag{3}$$

$$U_G = \begin{bmatrix} x_R - A_1.\Delta_{OG} - B_1.\Delta_{RO} & z_G \end{bmatrix}^T;$$
$$U_{Gr} = \begin{bmatrix} x_R + B_1.\Delta_{GrO} - B_1.\Delta_{RO} & z_G + A_2.\Delta_{OG} + B_2.\Delta_{GrO} \end{bmatrix}^T$$

$$U_F = \begin{bmatrix} x_R - A_1.\Delta_{OG} - B_1.\Delta_{RO} + A_1\Delta_{TG} + (z_G + A_2\Delta_{TG} - z_F).\tan(\theta+\psi) & z_F \end{bmatrix}^T \tag{4}$$
$$U_{G_f} = U_F + \begin{bmatrix} A_1.\Delta_{GfF} & A_2.\Delta_{GfF} \end{bmatrix}^T; \quad U_R = \begin{bmatrix} x_R & z_G + A_2.\Delta_{OG} + B_2.\Delta_{RO} \end{bmatrix}^T$$

Call L_r, L_f is the distance of SR and TF with L_{r0}, L_{f0} is the initial distance, we have:

$$L_r^2 = L_{SA}^2 + L_{RA}^2 - 2\cos(\gamma_0 + \varphi) \ , \quad L_f = \frac{(z_G + A_2\Delta_{TG} - z_F)}{\cos(\theta+\psi)} \tag{5}$$

Taking into account the rotation of the wheels, the kinetic energy expression of the system is:

$$T = \frac{1}{2}\left\{ m_G \dot{U}_G^T \dot{U}_G + m_{Gr} \dot{U}_{Gr}^T \dot{U}_{Gr} + I_{Gr}\dot{\varphi}^2 + m_{Gf} \dot{U}_{Gf}^T \dot{U}_{Gf} + I_G\dot{\theta}^2 + I_{Gf}\dot{\theta}^2 + 2m_R \dot{U}_R^T \dot{U}_R + 2m_F \dot{U}_F^T \dot{U}_F \right\} \tag{6}$$

and the potential energy is:

$$\Pi = \frac{1}{2}\left\{ C_f (L_f - L_{f0})^2 + C_r (L_r - L_{r0})^2 + C_{bf}(z_F - f(x_F) - z_F^0)^2 + C_{br}(z_R - f(x_R) - z_R^0)^2 \right\}$$
$$+ g(m_G z_G + m_{Gr} z_{Gr} + m_{Gf} z_{Gf} + m_R z_R + m_F z_F) \tag{7}$$

The energy dissipation function in the shock absorber and tire is expressed as:

$$W_d = \frac{1}{2}\left[k_f (\dot{L}_f)^2 + k_r (\dot{L}_r)^2 + k_{bf}(\dot{z}_F - \dot{f}(x_F))^2 + k_{br}(\dot{z}_R - \dot{f}(x_R))^2 \right] \tag{8}$$

in which: $\dot{f}(x_F) = \dfrac{\partial f}{\partial x} . \dfrac{dx}{dt}\Big|_{x=x_F}$ and $\dot{f}(x_R) = \dfrac{\partial f}{\partial x} . \dfrac{dx}{dt}\Big|_{x=x_R}$ (9)

2.3. External force

Neglect friction in the shafts and rolling resistance in contact with the ground. When moving, the aerodynamic force $\vec{F}_a = (-F_{ax}, F_{az})$ effect on the center of gravity $(x_G, z_G)^T$ of the suspension block, with $F_{ax} = \frac{1}{2}\rho.C_D.v^2.S$, $F_{az} = \frac{1}{2}\rho.C_L.v^2.S$, in which ρ is the air density, S is the area of the front surface and v is the speed of the vehicle, C_D and C_L is the coefficient of drag and aerodynamic lift. Virtual work of external force:

$$\delta W_e = -F_{ax}.\delta x_G + F_{az}.\delta z_G \tag{10}$$
$$\Rightarrow \delta W_e = F_{ax} dA_1.\Delta_{OG}\delta\theta + F_{ax} dB_1.\Delta_{RO}\delta\varphi + F_{az}.\delta z_G \tag{11}$$

$$Q_\theta = F_{ax}.dA_1.\Delta_{OG} \; ; \; Q_\varphi = F_{ax}dB_1.\Delta_{RO} \; ; \; Q_{z_G} = F_{az} \; ; \; Q_{z_F} = 0 \tag{12}$$

Hence there are generalized forces:

2.4. Equation of motion

Lagrange function of $L = T - \Pi$, with $q = \begin{bmatrix} \theta & \varphi & z_G & z_F \end{bmatrix}^T$ are the general Lagrange- coordinates. This leads to the below system of equations of motion:

$$\frac{d}{dt}\left(\frac{\partial T}{\partial \dot{q}_i}\right) = Q_i + \frac{\partial T}{\partial q_i} - \frac{\partial \Pi}{\partial q_i} - \frac{\partial W_d}{\partial \dot{q}_i} \tag{13}$$

Substituting the expressions (4),(6)-(8),(12) into (13) leads to a system of motion equations in the form of:

$$M(q,\dot{q}).\ddot{q} = P(q,\dot{q}) \tag{14}$$

By the symbols in Appendix A, the matrix M and P have the below forms:

$$M = \begin{bmatrix} A_{11} & A_{12} & A_{13} & A_{14} \\ A_{21} & A_{22} & A_{23} & A_{24} \\ A_{31} & A_{32} & A_{33} & A_{34} \\ A_{41} & A_{42} & A_{43} & A_{44} \end{bmatrix}; \quad P = \begin{bmatrix} \dfrac{\partial T}{\partial \theta} - \dfrac{\partial \Pi}{\partial \theta} - \dfrac{\partial W_d}{\partial \dot{\theta}} + Q_\theta - V_1 \\ \dfrac{\partial T}{\partial \varphi} - \dfrac{\partial \Pi}{\partial \varphi} - \dfrac{\partial W_d}{\partial \dot{\varphi}} + Q_\varphi - V_2 \\ \dfrac{\partial T}{\partial z_G} - \dfrac{\partial \Pi}{\partial z_G} - \dfrac{\partial W_d}{\partial \dot{z}_G} + Q_{z_G} - V_3 \\ \dfrac{\partial T}{\partial z_F} - \dfrac{\partial \Pi}{\partial z_F} - \dfrac{\partial W_d}{\partial \dot{z}_F} + Q_{z_F} - V_4 \end{bmatrix}; \quad \ddot{q} = \begin{bmatrix} \ddot{\theta} \\ \ddot{\varphi} \\ \ddot{z}_G \\ \ddot{z}_F \end{bmatrix}$$

The system of differential Eqs. (14) will be roughly solved by the Runge-Kutta method and performed on Matlab code. From the received values z_F, x_F will be calculated via $d_f = z_F - f(x_F) - z_F^0$. The front wheel tire grips the road surface if $d_f < 0$ and does not grip the road surface if $d_f \geq 0$.

3. Model survey and actual test

Let the coordinates of the initial center of gravity of the extinguishing media cluster to be as: $\left(x_M^0, z_M^0\right)$. The system of Eqs. (14) can be investigated with the parameters given in Table 2 and in the following cases:

- Coordinates $z_M^0 = z_{Gn}^0$ and x_M^0 will vary in the value (-0.3 , -0.15 , 0 , 0.15), (m)
- Vehicle speed changes in two different ways (as shown in Fig. 3)
- The mass of the fire-fighting equipment cluster m_M changes as 90, 110, 130 (kg). Notice that the mass of the suspension block is: $m_G = m_{Gn} + m_M$.

Table 2. Initial coordinates of motorcycle points and survey parameters

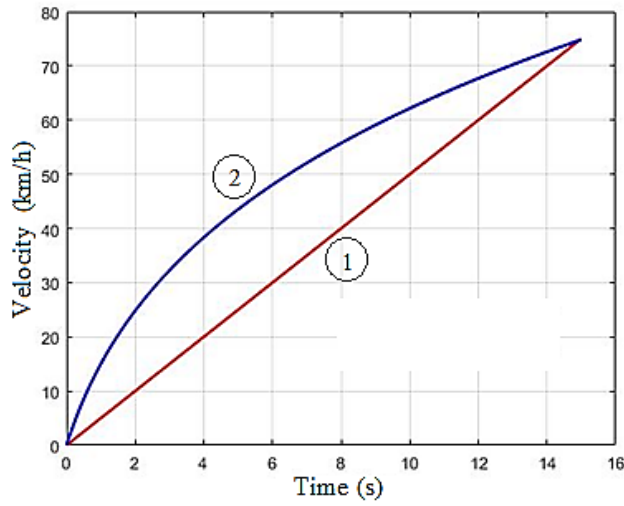| Symbol	Value	Symbol	Value	Symbol	Value
$\left(x_R^0, z_R^0\right)$	(0 , 0.306) [m]	m_{Gn}	172 [kg]	C_f	13 000 [N/m]
$\left(x_O^0, z_O^0\right)$	(0.421 , 0.391) [m]	m_{Gr}	8 [kg]	C_r	85 000 [N/m]
$\left(x_F^0, z_F^0\right)$	(1.275 , 0.296) [m]	m_{Gf}	4 [kg]	C_{bf}	172 916 [N/m]
$\left(x_T^0, z_T^0\right)$	(1.029 , 0.825) [m]	m_R	12 [kg]	C_{br}	180 664 [N/m]
$\left(x_S^0, z_S^0\right)$	(0.120 , 0.656) [m]	m_F	10 [kg]	k_f	1000 [Ns/m]
$\left(x_{G_r}^0, z_{G_r}^0\right)$	(0.250, 0.356) [m]	I_G	40 [kg m²]	k_r	4000 [Ns/m]
$\left(x_{G_f}^0, z_{G_f}^0\right)$	(1.175 , 0.512) [m]	I_{Gr}	0.3 [kgm²]	k_{bf}	150 [Ns/m]
$\left(x_{Gn}^0, z_{Gn}^0\right)$	(0.539, 0.759) [m]	I_{Gf}	0.1 [kgm²]	k_{br}	200 [Ns/m]
		C_d	0.3	$C_L C_L$	0.2

Fig. 3. Two ways of changing the speed of vehicle with time

When the vehicle is traveling on flat roads the bumpy height of the pavement is represented by the function $z = f(x)$ as below equation:

$$f(x) = \begin{cases} \dfrac{1}{2}H\left[1 - \cos\left(\dfrac{2\pi(x-L_0)}{L}\right)\right] & khi \quad L_0 < x < L_0 + L \\ 0 & khi \quad x \le L_0 , \quad L_0 + L \le x \end{cases} \tag{15}$$

Here, $H = 0.3(m)$ is the height of the bumper, $L = 0.5\ (m)$, $L_0 = 20\ (m)$ as shown in Fig. 4.
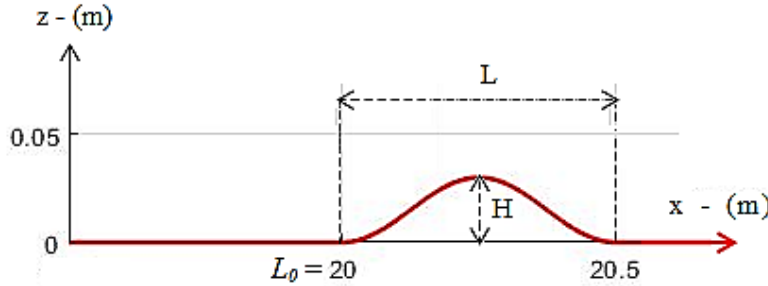
Fig. 4. Description of road surface bumper along the length.

When the front wheel is not in contact with the road surface the bumper is evaluated through the quantity $d_f = z_F - f(x_F) - R_F$, here (x_F, z_F) is the coordinates of the front wheel axis and R_F is the outer radius of the front tire. The front tire grips the road surface when $d_f < 0$ and does not contact the road surface when $d_f \ge 0$. Note that, there is always $d_f \ge -h_b$ with h_b the maximum deflection of the front tire. In this calculation, get $h_b = 0.02\ (m)$. Based on Fig. 3, two ways were considered to change the speed of the rear wheel of the vehicle. The equations for each graph can be written as:

Linear curve (1) shown in Fig. 3: $\quad v_R = \dfrac{25}{18}t , (m/s)$ \hfill (16)

Non-linear curve (2) shown in Fig. 3 : $v_R = \dfrac{505}{18}\left[(t+1)^{\frac{1}{5}} - 1\right] , (m/s)$ \hfill (17)

By considering the mass of instrument cluster $m_M = 90\ kg$ on two types of flat road with and without burrs and giving two ways of changing the speed (shown in Fig. 3), the variations of d_f value can be obtained for variable x_M value. Two different cases (1) flat road and (2) rad with barrier are considered for the analyses. Figs. 5 and 6 show the variations of d_f

on a flat road surface. Based on these two Figures it is seen that the vehicle's ability to grip the road is reduced when the x_M value is smaller (i.e. the closer the vehicle cluster is mounted to the rear). Also, with the speed change method (1), the vehicle grips the road better than the speed change method (2). With the method (1) the vehicle grips the road at $x_M \geq 0$ for all speeds (Fig.5), but with the speed change of method (2) where $x_M = 0$, the front wheel does not stick to the road surface when the vehicle is at a speed of > 50km/h (as seen from Fig. 6). This is because the velocity change in mode (2) has a larger acceleration than the acceleration when the velocity changes in mode (1).
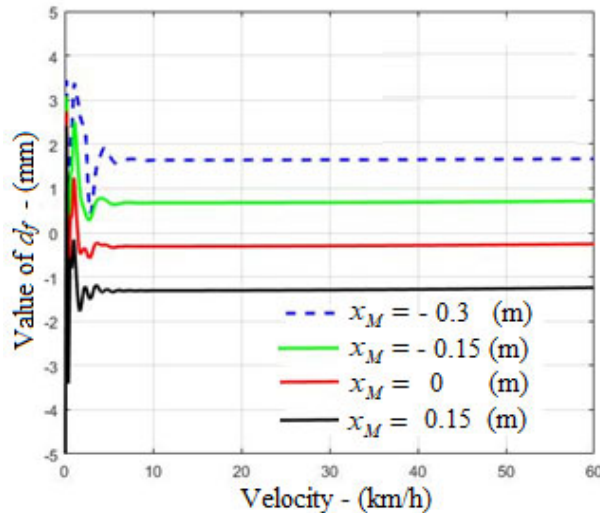

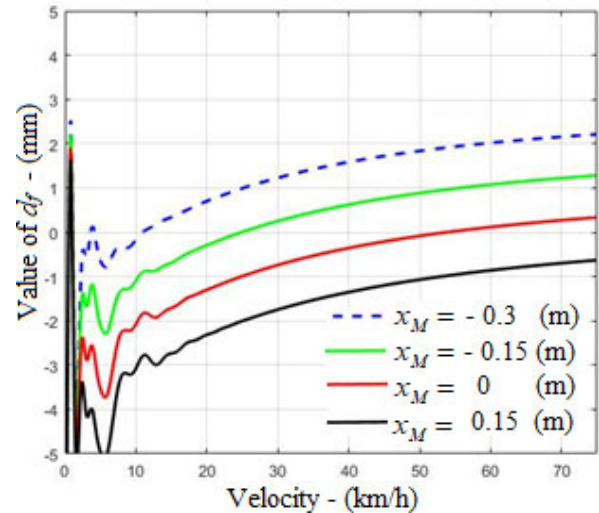**Fig. 5**. Graph d_f versus velocity according to Eq. (16) No burrs: f(x) = 0

Fig. 6. Graph of d_f with velocity according to Eq. (17). No burrs: f(x) = 0

Figs. 7 and 8 also present the variations of d_f on a road with a 30cm high and 0.5m wide barrier (defined earlier in Fig. 4). In such case all vehicles should pass at a speed of greater than 25 km/h.
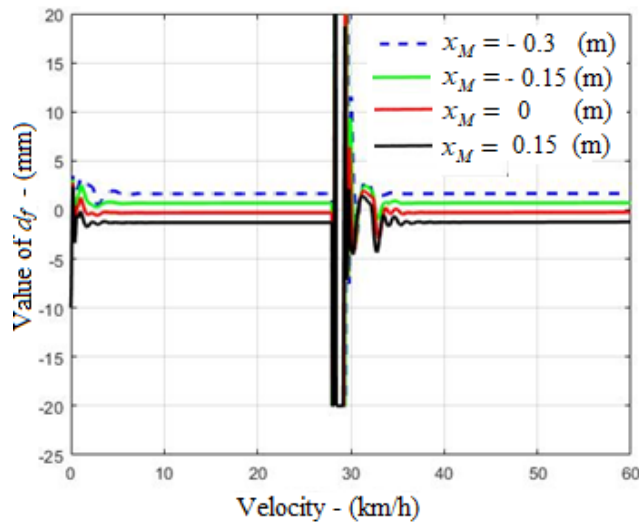

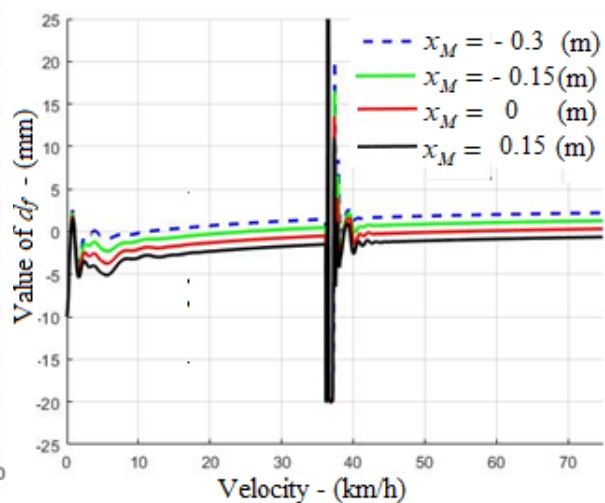**Fig. 7.** Graph of d_f with velocity according to Eq. (16). With bumper: $f(x) > 0$

Fig. 8. Graph d_f versus velocity according to Eq. (17). With bumper: $f(x) > 0$

The effect of mass of instrument cluster (m_M) on the variations of d_f is also investigated in Fig. 9 for different speeds of vehicle and also two values of $x_M = 0$ and $x_M = 0.15(m)$. According to this Figure, when the vehicle runs on a flat road without burrs, (coordinates $x_M = 0.15(m)$), the front wheel of the car still grips the road at all speeds < 70km/h, but the mass of the instrument cluster can carry up to 130 kg, while it can only carry 90 kg if $x_M = 0$.
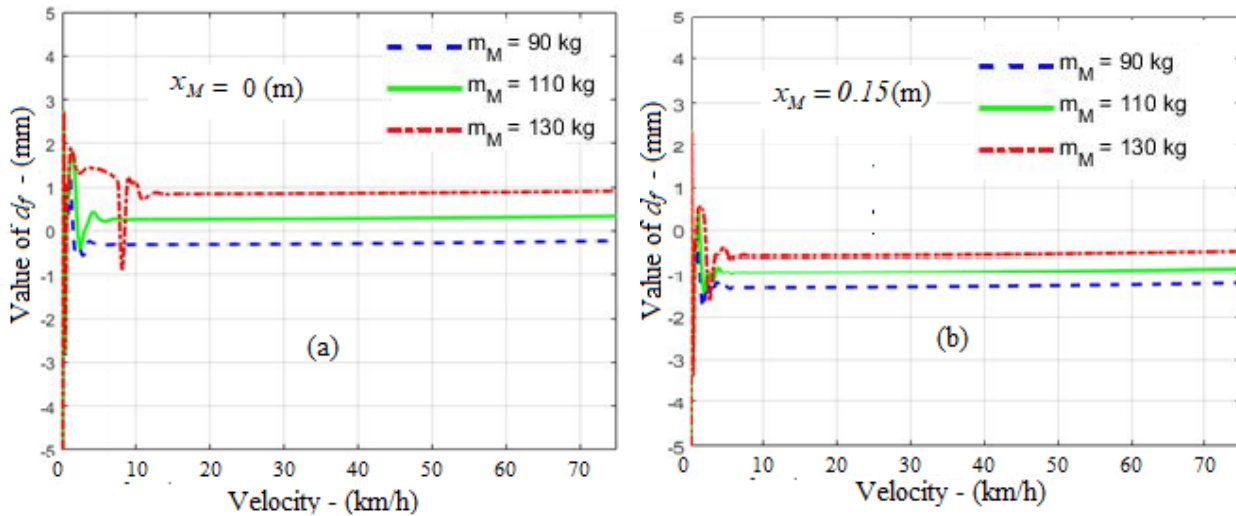
Fig. 9. Graph d_f versus velocity (Eq.16) without obstacle: f(x) =0 and for different masses of instrument cluster m_M = 90, 110, 130 (kg) ; **(a)** $x_M = 0(m)$, **(b)** $x_M = 0.15m$

3.1 Practical test

In order to examine the above-mentioned computational model in practice, it is necessary to use measuring and recording equipment during the experiment. A vehicle speedometer obtains the vehicle speed over time in numerical form. A wire-type pressure gauge "tenzo" is affixed to the surface of the tire in the road contact area. Vehicle speed and tire pressure are recorded synchronously with time. From the pressure value P_f on the front tire one can calculate the settlement parameter ($d_f = \dfrac{P_f}{C_{bf}}$) of the front tire on the road. If the pressure gauge value is zero, it corresponds to $d_f \geq 0$, then the front tire of the vehicle is not gripping the road surface. Testing equipment includes 02 wireless transceivers and signal amplifiers, 01 set of Encoder E6B2-CWZ6C, 01 set of Spider8 (with 8 signal reception channels), 01 computer with specialized Catman software for Spider 8. The required testing equipment and setup are shown and illustrated in Figs. 10 and 11.
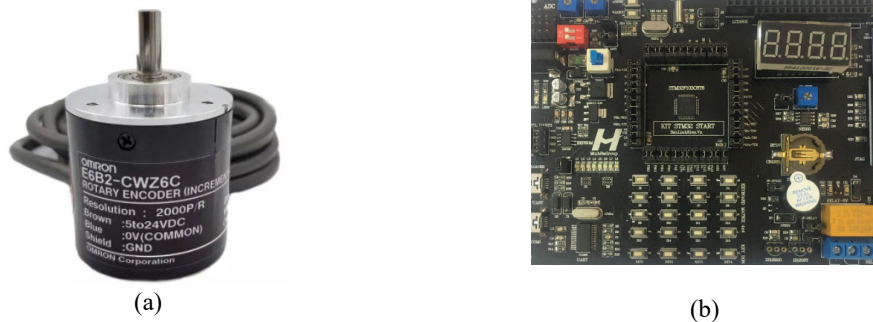

(a)   (b)

Fig. 10. Encoder and Central Processing Unit
(a) Encoder E6B2-CWZ6C with output 2000 square pulses/revolution.
(b) Central processor using STM32 microcontroller with kid's board programming in C . language
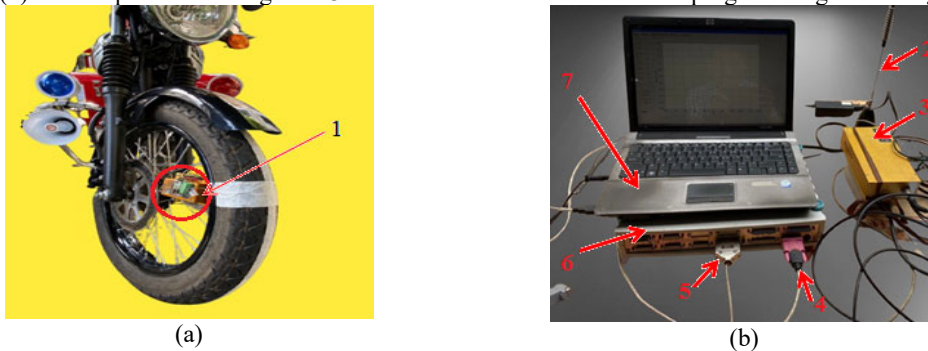

(a)   (b)

Fig. 11. Arrangement of testing equipment for measuring wheel traction

1)- The first wireless transmitter (with an input connected to the pressure gauge "tenzo" glued to the outside of the front tire) mounted on the spokes, rotating with the wheel; (2)- The antenna receives the signal from the transmitter; (3)- Amplifier of the received signal; (4)- The signal port from the amplifier to Spider8 according to the principle of parallel signal transmission; (5)-Signal port from Spider8 to PC according to the principle of serial signal transmission (RS-485); (6) - Spider8; (7) – Computer.

3.2.2 Arrange for the actual testing of the model

The Encoder was fixed on the vehicle and coaxial with the front wheel (via the speedometer wire). The output signal of the Encoder was connected to a second wireless transmitter located on the vehicle.

Signals transmitted from two wireless transmitters (with two different frequencies) are received through two antennas to two signal amplifiers (which are part of the Spider 8)'s peripherals. The signal from the amplifier is fed to the Spider 8 through the parallel communication port (8 bits). Next Spider 8 is communicated with the PC through the parallel communication port (RS-485) as shown in Fig.11(b).

Catman specialized software for Spider 8 is designed to be able for storing the data and exporting the data to Excel or Matlab files. From Spider 8's dedicated Catman software the time to count pulses was set to $t = 1(s)$. The velocity formula was calculated as follows: $v = \dfrac{n}{t.2000}$ (rpm), n is the total number of pulses counted. Testing data are recorded in Appendix B, in which the quantities: t, V_R_TN, d_f_TN are time, speed and d_f calculated through testing, respectively. The discrete data of the V_R_TN velocity measured through the experiment (described by the "+" signs in Fig.12) to be used to test the theoretical computational model, they need to be described as below: (i) defining of a dependent function t (described by a continuous curve in Fig.12); (ii) using the least squares method, the vehicle speed is expressed as a quadratic function V_R_QH dependent on t; (iii) applying the V_R_QH acceleration rule to the theoretical model, after the calculation, the corresponding d_f_LT value is obtained and finally (iv) comparing the correlation coefficient between two ranges of values d_f_TN and d_f_LT to draw conclusions about whether the theoretical model is consistent with reality or not. The test was performed with a device with a mass of 90 kg, the V_R_TN velocity changed according to the rule of figure 12 (Fig.12a – with $x_M = 0.15m$, Fig.12b - with $x_M = 0$)
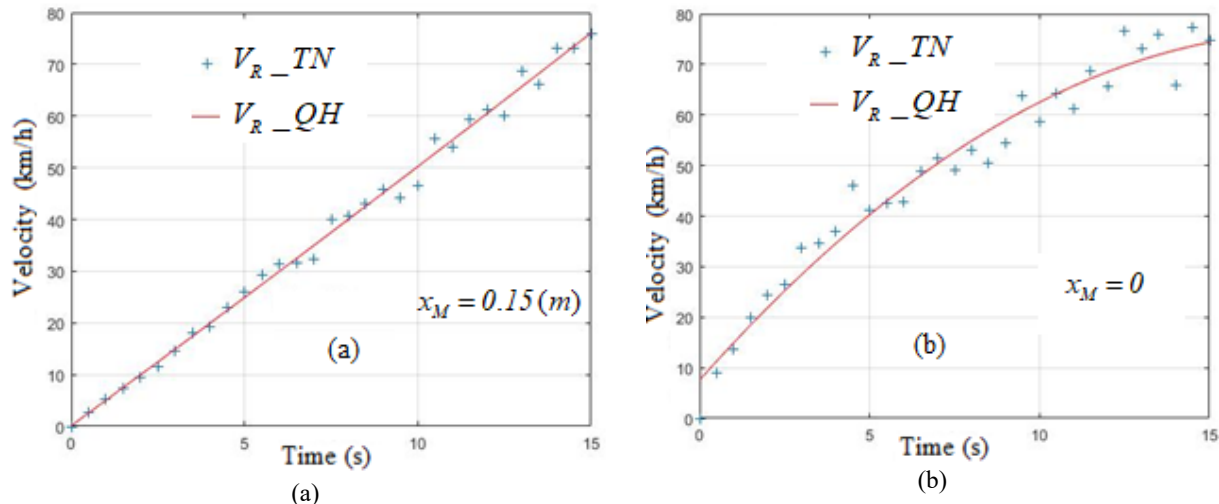

Fig. 12. V_R_TN test velocity over time; (a) $x_M = 0.15m$, (b) $x_M = 0$.

Corresponding to the measured V_R_TN values during the experiment, by means of least squares, the V_R_QH formula that describes the rule of V_R_TN over time is obtained:

With figure 12a: $V_R\_QH = 0.010273t^2 + 4.91019t + 0.102312\ (km/h)$ (18)

With figure 12b: $V_R\_QH = -0.20847\ t^2 + 7.579875t + 7.576897\ (km/h)$ (19)

Fig. 13 presents the results of df versus velocity obtained from the tests for two cases of (a) $x_M = 0.15m$ and (b) $x_M = 0$. Note that, when testing; only $d_f < 0$ values were recorded, so in Fig.13b, the graph of d_f_TN only reached $V_R = 50\ km/h$ because then the front wheel did not stick to the road surface anymore.
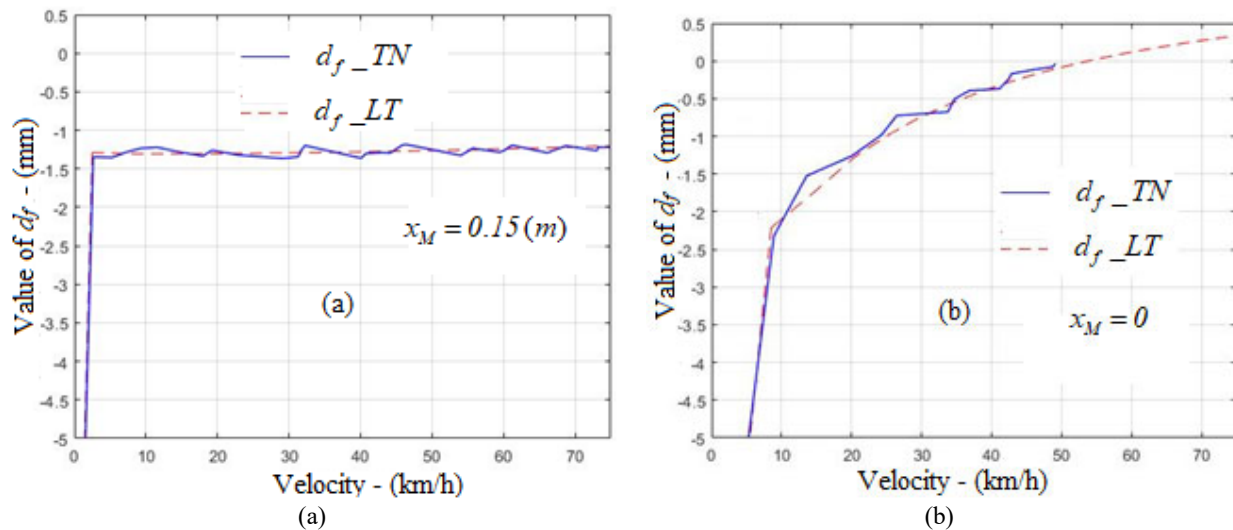
Fig. 13. *The d_f_TN measured from the assay and the d_f_LT value calculated by the model;* (a) $x_M = 0.15\,m$, (b)

$$x_M = 0$$

From the data in Appendix B, it is found that the range of values of d_f_TN and d_f_LT have a correlation coefficient of 0.99 for both cases $x_M = 0.15\,m$ and $x_M = 0$. This proves that the flat motion model of the motorcycle given is consistent with reality. Through model survey and actual test, it was found that the front wheel will always stick to the road surface when the vehicle is running and overcome the obstacle with a height of $H = 0.3\,m$ with speeds $v \leq 70\,km/h$ and mass $m_M \leq 130\,kg$. The equipment cluster carried must satisfy the conditions: $x_M \geq 0.15\,m$. Due to the design of the vehicle, the value z_M^0 cannot be changed and the value x_M^0 cannot be larger than $0.15m$. Therefore, the best location for mounting the device assembly is $x_M = 0.15\,m$ and $z_M = z_M^0$.

4. Conclusion

The firefighting and rescue motorcycle is designed on the basis of the Kawasaki W175 2019 base motorcycle when installing a cluster of firefighting and rescue equipment. Applying the plane dynamics model for two-wheeled vehicles, the system of differential equations of motion is established. The survey of the system of equations performed on Matlab gives the results on the best location to install the instrument cluster to keep the wheels on the road at all speeds $v \leq 70\,km/h$ with the mass of the instrument cluster $m_M \leq 130\,kg$. The test results show the suitability and reliability of the model with reality. The planar dynamics model stated in the paper can be applied to calculate the traction of two-wheeled vehicles in flat motion.

References

Benini, C., Gadola, M., Chindamo, D., Uberti, S., Marchesin, F. P., & Barbosa, R. S. (2017). The influence of suspension components friction on race car vertical dynamics. *Vehicle system dynamics, 55*(3), 338-350.

Chindamo, D., Lenzo, B., & Gadola, M. (2018). On the vehicle sideslip angle estimation: a literature review of methods, models, and innovations. *Applied Sciences, 8*(3), 355.

Cossalter V. (2006). Motorcycle dynamics; 2nd edition. ISBN 978-1430308614.

Cossalter, V., Doria, A., & Lot, R. (2000). Optimum suspension design for motorcycle braking. *Vehicle System Dynamics, 34*(3), 175-198.

Hossack, N.H. (1983). *Motorcycle suspension*. GB Patent No. 2121364A. Published 21 Dec. 1983.

Marchesin, F. P., Barbosa, R. S., Gadola, M., & Chindamo, D. (2018). High downforce race car vertical dynamics: aerodynamic index. *Vehicle System Dynamics, 56*(8), 1269-1288.

Mavroudakis, B., & Eberhard, P. (2006). Analysis of alternative front suspension systems for motorcycles. *Vehicle system dynamics, 44*(sup1), 679-689.

Sharma, A., & Limebeer, D. J. (2012). Dynamic stability of an aerodynamically efficient motorcycle. *Vehicle system dynamics, 50*(8), 1319-1340.

Sharp, R. S. (2006). Single-track vehicle modeling and control: Bicycles, motorcycles, and models. *IEEE Control Systems, 26* (5), 34-61.

Sharp, R. S. (2008). On the stability and control of the bicycle. *Applied Mechanics Reviews, 61*(1-6): 0608031-06080324.

Sharp, R.S. (1985). The Lateral Dynamics of Motorcycles and Bicycles. *Vehicle System Dynamics, 14*(4-6): 265-283.

Sharp, R. S. (1976). The dynamics of single track vehicles. *Vehicle system dynamics, 5*(1-2), 67-77.

Sharp, R. S. (2001). Stability, control and steering responses of motorcycles. *Vehicle system dynamics, 35*(4-5), 291-318.

Sharp, R. S. (2012). Rider control of a motorcycle near to its cornering limits. *Vehicle system dynamics, 50*(8), 1193-1208.

Sharp, R. S., Evangelou, S., & Limebeer, D. J. (2004). Advances in the modelling of motorcycle dynamics. *Multibody system dynamics, 12*(3), 251-283.

Tanelli, M., Corno, M., & Saveresi, S. (2014). *Modelling, simulation and control of two-wheeled vehicles.* John Wiley & Sons.

Weir, D. H. (1977). Motorcycle Dynamics and Rider Control. *Vehicle System Dynamics, 6*(2-3), 187-190.

Zanarini, A., & Brugnoni, E. (2012). Frequency analysis of a motorbike under motion conditions. In ISMA2012-USD2012 Conferences, Volume: Multi-Body Dynamics and Control.

Zhu, S., Murakami, S., & Nishimura, H. (2012). Motion analysis of a motorcycle taking into account the rider's effects. *Vehicle system dynamics, 50*(8), 1225-1245.

Appendix A

$$T_1 = \left\{ dA_1.\left(\Delta_{TG} - \Delta_{OG}\right) + dA_2 \Delta_{TG} \tan(\theta+\psi) + \left[z_G + A_2\Delta_{TG} - z_F\right].\left[1 + \tan^2(\theta+\psi)\right] \right\}$$

$$T_2 = T_1 + dA_1.\Delta_{GfF}$$

$$p_1 = A_1 \Delta_{OG} \dot{\theta}^2 + B_1.\Delta_{RO} \dot{\varphi}^2 + \dot{v}_R \quad ; \quad p_2 = B_1.\left(\Delta_{RO} - \Delta_{GrO}\right)\dot{\varphi}^2 + \dot{v}_R \quad ; \quad p_3 = -A_2.\Delta_{OG}\dot{\theta}^2 - B_2.\Delta_{GrO}\dot{\varphi}^2 \ ;$$

$$p_4 = -A_2.\Delta_{OG}\dot{\theta}^2 - B_2.\Delta_{RO}\dot{\varphi}^2 \ ; \quad p_5 = T_1 \quad ; \quad p_6 = B_1.\Delta_{RO}\dot{\varphi}^2 + \left[\dot{z}_G - \dot{z}_F\right].\left(1 + \tan^2(\theta+\psi)\right)\dot{\theta} + \dot{T}_1\dot{\theta} + \dot{v}_R$$

$$A_{11} = m_G\left(dA_1.\Delta_{OG}\right)^2 + m_{Gr}\left(dA_2.\Delta_{OG}\right)^2 + 2m_F p_5 T_1 + m_{Gf}\left[\left(p_5 + dA_1.\Delta_{GfF}\right)T_2 + \left(dA_2.\Delta_{GfF}\right)^2\right] +$$

$$+ 2m_R\left(dA_2.\Delta_{OG}\right)^2 + \left(I_G + I_{Gf}\right)$$

$$A_{12} = m_G dB_1.\Delta_{RO} dA_1.\Delta_{OG} + m_{Gr} dB_2.\Delta_{GrO} dA_2.\Delta_{OG} - 2m_F dB_1.\Delta_{RO}.T_1 - m_{Gf} dB_1.\Delta_{RO}.T_2 + 2m_R dB_2.\Delta_{RO} dA_2.\Delta_{OG}$$

$$A_{13} = m_{Gr} dA_2.\Delta_{OG} + 2m_F \tan(\theta+\psi)T_1 + m_{Gf}\tan(\theta+\psi)T_2 + 2m_R dA_2.\Delta_{OG}$$

$$A_{14} = m_{Gf} dA_2.\Delta_{GfF} - 2m_F \tan(\theta+\psi)T_1 - 2m_{Gf}\tan(\theta+\psi)T_2$$

$$V_1 = m_G p_1 dA_1.\Delta_{OG} + m_G \dot{U}_G^{(1)} A_1.\Delta_{OG}\dot{\theta} + m_{Gr} p_3 dA_2.\Delta_{OG} - m_{Gr}\dot{U}_{Gr}^{(2)} A_2.\Delta_{OG}\dot{\theta} + 2m_F p_6 T_1 + 2m_F \dot{U}_F^{(1)}.\dot{T}_1$$

$$+ m_{Gf}\left[p_6 - A_1.\Delta_{GfF}\dot{\theta}^2\right]T_2 + m_{Gf}\dot{U}_{Gf}^{(1)}\dot{T}_2 - m_{Gf} A_2.\Delta_{GfF}\dot{\theta}^2 dA_2.\Delta_{GfF} - m_{Gf}\dot{U}_{Gf}^{(2)} A_2.\Delta_{GfF}\dot{\theta}$$

$$+ 2m_R p_4 dA_2.\Delta_{OG} - 2m_R\dot{U}_R^{(2)} A_2.\Delta_{OG}\dot{\theta}$$

$$A_{21} = \left[m_G dA_1.\Delta_{OG} - m_{Gf}\left(p_5 + dA_1.\Delta_{GfF}\right) - 2m_F p_5\right]dB_1.\Delta_{RO} + m_{Gr} dA_2.\Delta_{OG} B_2\Delta_{GrO} + 2m_R dA_2.\Delta_{OG} dB_2.\Delta_{RO}$$

$$A_{22} = \left[m_G + m_{Gf} + 2m_F\right]\left(dB_1.\Delta_{RO}\right)^2 + m_{Gr}\left[dB_1.\left(\Delta_{GrO} - \Delta_{RA}\right)\right]^2 + m_{Gr} dB_2.\Delta_{GrO} B_2\Delta_{GrO} + 2m_R\left(dB_2.\Delta_{RO}\right)^2 + I_{Gr}$$

$$A_{23} = -\tan(\theta+\psi)\left(m_{Gf} + 2m_F\right)dB_1.\Delta_{RO} + m_{Gr} B_2\Delta_{GrO} + 2m_R dB_2.\Delta_{RO}$$

$$A_{24} = \tan(\theta+\psi)\left(m_{Gf} + 2m_F\right)dB_1.\Delta_{RO}$$

$$V_2 = \left\{m_{Gf}\left[A_1.\Delta_{GfF}\dot{\theta}^2 - p_6\right] - 2m_F p_6 - m_G p_1\right\}dB_1.\Delta_{RO} + \left(m_G \dot{U}_G^{(1)} + m_{Gf}\dot{U}_{Gf}^{(1)} + 2m_F\dot{U}_F^{(1)}\right)B_1.\Delta_{RO}\dot{\varphi}$$

$$+ m_{Gr}\left[+p_2\right]dB_1\left(\Delta_{GrO} - \Delta_{RO}\right) - m_{Gr}\dot{U}_{Gr}^{(1)} B_1\left(\Delta_{GrO} - \Delta_{RO}\right)\dot{\varphi}$$

$$+ m_{Gr}\left[p_3\right]B_2\Delta_{GrO} + m_{Gr}\dot{U}_{Gr}^{(2)} dB_2\Delta_{GrO}\dot{\varphi}$$

$$+ 2m_R\left[p_4\right]dB_2.\Delta_{RO} - 2m_R\dot{U}_R^{(2)} B_2.\Delta_{RO}\dot{\varphi}$$

$$A_{31} = \left[m_{Gr} + 2m_R\right]dA_2.\Delta_{OG} + \tan(\theta+\psi)\left[m_{Gf}\left(p_5 + dA_1.\Delta_{GfF}\right) + 2m_F p_5\right]$$

$$A_{32} = dB_2.\left[m_{Gr}\Delta_{GrO} + 2m_R\Delta_{RO}\right] - \left[m_{Gf} + 2m_F\right]\tan(\theta+\psi)dB_1.\Delta_{RO}$$

$$A_{33} = m_G + m_{Gr} + 2m_R + \left[m_{Gf} + 2m_F\right]\tan^2(\theta+\psi)$$

$$A_{34} = -\left[m_{Gf} + 2m_F\right]\tan^2(\theta+\psi)$$

$$V_3 = m_{Gr} p_3 + 2m_R p_4 + m_{Gf} \tan(\theta+\psi)\left[p_6 - A_1.\Delta_{GfF}\dot{\theta}^2 \right] \qquad + 2m_F \tan(\theta+\psi) p_6 +$$

$$+ \left[m_{Gf}\dot{U}_{Gf}^{(1)} + 2m_F\dot{U}_F^{(1)} \right]\left[1 + \tan^2(\theta+\psi) \right]\dot{\theta}$$

$$A_{41} = \left\{ -\tan(\theta+\psi)\left[m_{Gf}\left(p_5 + dA_1.\Delta_{GfF} \right) + 2m_F p_5 \right] + m_{Gf} dA_2.\Delta_{GfF} \right\}$$

$$A_{42} = \left\{ \left[m_{Gf} + 2m_F \right]\tan(\theta+\psi)dB_1.\Delta_{RO} \right\} \quad ; \quad A_{43} = \left\{ -\left[m_{Gf} + 2m_F \right]\tan^2(\theta+\psi) \right\}$$

$$A_{44} = \left\{ \left[m_{Gf} + 2m_F \right]\tan^2(\theta+\psi) + m_{Gf} + 2m_F \right\}$$

$$V_4 = \tan(\theta+\psi)\left[m_{Gf} A_1.\Delta_{GfF}\dot{\theta}^2 - p_6\left(m_{Gf} + 2m_F \right) \right] - \left[m_{Gf}\dot{U}_{Gf}^{(1)} + 2m_F\dot{U}_F^{(1)} \right]\left[1 + \tan^2(\theta+\psi) \right]\dot{\theta} - m_{Gf} A_2.\Delta_{GfF}\dot{\theta}^2$$

$$\frac{\partial T}{\partial \theta} = m_G \dot{U}_G^{(1)} A_1.\Delta_{OG}\dot{\theta} - m_{Gr}\dot{U}_{Gr}^{(2)} A_2.\Delta_{OG}\dot{\theta} + m_{Gf}\dot{U}_{Gf}^T \frac{\partial}{\partial\theta}\left(\dot{U}_{Gf} \right) - 2m_R\dot{U}_R^{(2)} A_2.\Delta_{OG}\dot{\theta} + 2m_F\dot{U}_F^T \frac{\partial}{\partial\theta}\left(\dot{U}_F \right)$$

$$\frac{\partial T}{\partial \varphi} = m_G \dot{U}_G^{(1)} B_1.\Delta_{RO}\dot{\varphi} + m_{Gr}\dot{U}_{Gr}^T \left[\begin{matrix} B_1.(\Delta_{RO} - \Delta_{GrO})\dot{\varphi} \\ -B_2\Delta_{GrO}\dot{\varphi} \end{matrix} \right] - 2m_R\dot{U}_R^{(2)} B_2.\Delta_{RO}\dot{\varphi} + \left(2m_F\dot{U}_F^{(1)} + m_{Gf}\dot{U}_{Gf}^{(1)} \right) B_1.\Delta_{RO}\dot{\varphi}$$

$$\frac{\partial T}{\partial z_G} = \left(2m_F\dot{U}_F^{(1)} + m_{Gf}\dot{U}_{Gf}^{(1)} \right)\left[1 + \tan^2(\theta+\psi) \right]\dot{\theta} \quad ; \quad \frac{\partial T}{\partial z_F} = -\left(2m_F\dot{U}_F^{(1)} + m_{Gf}\dot{U}_{Gf}^{(1)} \right)\left[1 + \tan^2(\theta+\psi) \right]\dot{\theta}$$

$$\frac{\partial \Pi}{\partial \theta} = C_f\left(L_f - L_{f0} \right).\left[L_f.\tan(\theta+\psi) + \frac{dA_2\Delta_{TG}}{\cos(\theta+\psi)} \right] + C_{br}\left(z_R - f(x_R) - z_R^0 \right)(dA_2.\Delta_{OG}) -$$

$$- C_{bf}\left(z_F - f(x_F) - z_F^0 \right)\frac{\partial f(x_F)}{\partial x}.\frac{\partial x_F}{\partial \theta} + g.dA_2\left(m_{Gr}.\Delta_{OG} + m_{Gf}.\Delta_{GfF} + m_R.\Delta_{OG} \right)$$

$$\frac{\partial \Pi}{\partial \varphi} = C_r\left(L_r - L_{r0} \right)\frac{\sin(\gamma_0 + \varphi)}{L_r} - C_{bf}\left(z_F - f(x_F) - z_F^0 \right)\frac{\partial f(x_F)}{\partial x} dB_1.\Delta_{RO}$$

$$+ g.dB_2\left(m_{Gr}.\Delta_{GrO} + m_{Gf}.\Delta_{GfF} + m_R.\Delta_{RO} \right) + C_{br}\left(z_R - f(x_R) - z_R^0 \right)(dB_2.\Delta_{RO})$$

$$\frac{\partial \Pi}{\partial z_G} = C_f\left(L_f - L_{f0} \right)\frac{1}{\cos(\theta+\psi)} - C_{bf}\left(z_F - f(x_F) - z_F^0 \right)\frac{\partial f(x_F)}{\partial x}.\tan(\theta+\psi) +$$

$$+ C_{br}\left(z_R - f(x_R) - z_R^0 \right) + m_G.g + m_{Gr}.g. + m_R.g$$

$$\frac{\partial \Pi}{\partial z_F} = -C_f\left(L_f - L_{f0} \right)\frac{1}{\cos(\theta+\psi)} + C_{bf}\left(z_F - f(x_F) - z_F^0 \right).\left(1 + \frac{\partial f(x_F)}{\partial x}.\tan(\theta+\psi) \right) + m_{Gf}.g + m_F.g$$

$$\frac{\partial W_d}{\partial \dot{\theta}} = k_f\dot{L}_f\left(\frac{dA_2.\Delta_{TG}}{\cos(\theta+\psi)} + \frac{(z_G + A_2\Delta_{TG} - z_F)}{\cos(\theta+\psi)}\tan(\theta+\psi) \right) -$$

$$- k_{bf}\left(\dot{z}_F - \dot{f}(x_F) \right)\frac{\partial f(x_F)}{\partial x}\frac{\partial \dot{x}_F}{\partial \dot{\theta}} + k_{br}\left(\dot{z}_R - \dot{f}(x_R) \right)dA_2.\Delta_{OG}$$

$$\frac{\partial W_d}{\partial \dot{\varphi}} = k_r\dot{L}_r\frac{\sin(\gamma_0 + \varphi)}{L_r} - k_{bf}\left(\dot{z}_F - \dot{f}(x_F) \right)\frac{\partial f(x_F)}{\partial x}.\frac{\partial \dot{x}_F}{\partial \dot{\varphi}} + k_{br}\left(\dot{z}_R - \dot{f}(x_R) \right)dB_2.\Delta_{RO}$$

$$\frac{\partial W_d}{\partial \dot{z}_G} = k_f\dot{L}_f\frac{1}{\cos(\theta+\psi)} - k_{bf}\left(\dot{z}_F - \dot{f}(x_F) \right)\frac{\partial f(x_F)}{\partial x}\frac{\partial \dot{x}_F}{\partial \dot{z}_G} + k_{br}\left(\dot{z}_R - \dot{f}(x_R) \right)$$

$$\frac{\partial W_d}{\partial \dot{z}_F} = -k_f\dot{L}_f\frac{1}{\cos(\theta+\psi)} + k_{bf}\left(\dot{z}_F - \dot{f}(x_F) \right)\left\{ 1 - \frac{\partial f(x_F)}{\partial x}\frac{\partial \dot{x}_F}{\partial \dot{z}_F} \right\}$$

Appendix B

t	$x_M = 0.15\ (m)$						$x_M = 0$	
	d_f_TN	V_R_QH	d_f_LT	d_f_LT	V_R_TN	d_f_TN	V_R_QH	d_f_LT
(s)	(km/h)	(mm)	(km/h)	(mm)	(km/h)	(mm)	(km/h)	(mm)
0	0.0	-10.15	0.1	-10.00	0.0	-8.91	7.6	-10.00
0.5	2.6	-1.35	2.6	-1.29	8.9	-2.32	11.3	-2.21
1	5.3	-1.35	5.0	-1.30	13.6	-1.52	14.9	-1.71
1.5	7.3	-1.28	7.5	-1.31	20.0	-1.26	18.5	-1.28
2	9.3	-1.23	10.0	-1.31	24.3	-0.98	21.9	-1.00
2.5	11.6	-1.22	12.4	-1.31	26.4	-0.73	25.2	-0.80
3	14.7	-1.28	14.9	-1.31	33.8	-0.68	28.4	-0.64
3.5	18.0	-1.34	17.4	-1.31	34.7	-0.50	31.6	-0.51
4	19.2	-1.26	19.9	-1.30	36.9	-0.39	34.6	-0.41
4.5	22.9	-1.32	22.4	-1.30	46.1	-0.37	37.5	-0.32
5	26.0	-1.34	24.9	-1.30	41.1	-0.23	40.3	-0.25
5.5	29.2	-1.37	27.4	-1.30	42.5	-0.17	43.0	-0.19
6	31.3	-1.34	29.9	-1.29	42.8	-0.11	45.6	-0.13
6.5	31.7	-1.26	32.5	-1.29	48.8	-0.08	48.0	-0.08
7	32.2	-1.20	35.0	-1.29	51.4	-0.04	50.4	-0.04
7.5	40.1	-1.36	37.5	-1.28	49.1		52.7	0.00
8	40.8	-1.30	40.0	-1.28	53.1		54.9	0.04
8.5	43.0	-1.29	42.6	-1.28	50.5		56.9	0.07
9	45.9	-1.29	45.1	-1.27	54.5		58.9	0.10
9.5	44.2	-1.19	47.7	-1.27	63.8		60.8	0.13
10	46.4	-1.18	50.2	-1.26	58.7		62.5	0.15
10.5	55.7	-1.33	52.8	-1.26	64.2		64.2	0.18
11	54.0	-1.23	55.4	-1.25	61.2		65.7	0.20
11.5	59.4	-1.28	57.9	-1.25	68.8		67.2	0.22
12	61.2	-1.26	60.5	-1.24	65.6		68.5	0.24
12.5	60.1	-1.19	63.1	-1.24	76.6		69.8	0.26
13	68.7	-1.29	65.7	-1.23	73.1		70.9	0.27
13.5	66.1	-1.20	68.3	-1.22	75.9		71.9	0.29
14	73.1	-1.26	70.9	-1.22	66.0		72.8	0.30
14.5	73.2	-1.22	73.5	-1.21	77.3		73.7	0.32
15	75.9	-1.22	76.1	-1.20	74.9		74.4	0.33